

Force-Based Adaptive Deposition in Multi-Axis Additive Manufacturing: Low Porosity for Enhanced Strength

Yuming Huang^{a,*}, Renbo Su^{a,*}, Kun Qian^a, Tianyu Zhang^a, Yongxue Chen^a, Tao Liu^a, Guoxin Fang^b, Weiming Wang^a, Charlie C.L. Wang^{a,**}

^a*Department of Mechanical and Aerospace Engineering, The University of Manchester, Manchester, M13 9PL, United Kingdom*

^b*Department of Mechanical and Automation Engineering, The Chinese University of Hong Kong, Shatin, N.T., Hong Kong, China*

Abstract

Multi-axis additive manufacturing enhances mechanical strength by aligning printed layers with principal stress directions. However, this benefit introduces a key challenge: non-uniform layer thickness becomes inevitable due to surface curvature and deposition angle variations. Moreover, unpredictable errors in material deposition – such as inaccurate extrusion control, collapse of earlier deposited layers, or machine malfunctions – can accumulate throughout the build. These issues are difficult to model accurately in advance, making purely offline planning impractical for ensuring consistent print quality, especially in complex geometries. To address this issue, we propose a force-based adaptive deposition method that actively minimizes porosity during filament-based multi-axis AM. Our closed-loop control strategy dynamically adjusts the printhead feedrate based on real-time force feedback, while maintaining constant extrusion speed. Unlike geometry-driven offline planning approaches, our method compensates for thickness variation and process uncertainties, resulting in improved filament bonding. Experiments show up to a 72.1% increase in failure load compared to baseline methods, with similar or lower part weights. The approach also enhances robustness against extrusion irregularities, ensuring more consistent mechanical performance.

Keywords: Adaptive Deposition; Force-Based; Porosity Control; Mechanical Strength; Multi-Axis Additive Manufacturing.

*These authors contributed equally to this work

**Corresponding authors. E-mail: charlie.wang@manchester.ac.uk

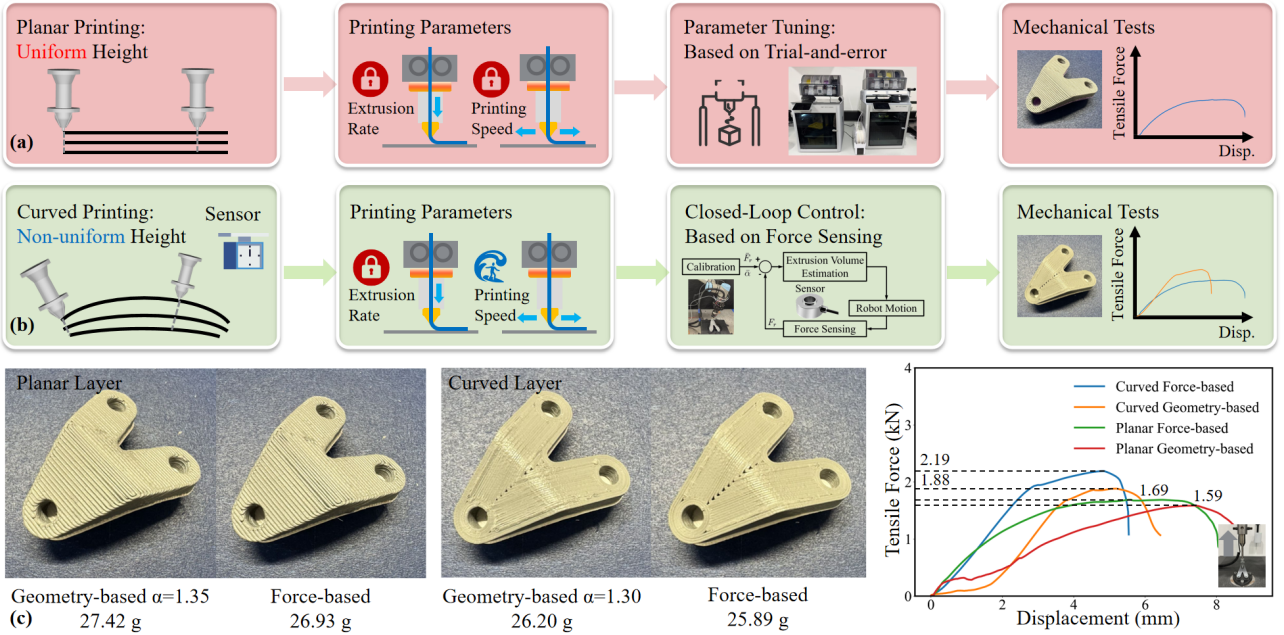


Figure 1: Advantage and challenge of multi-axis 3D printing with curved layers. (a) In conventional planar 3D printing, the fixed layer height allows for a *constant* optimal extrusion rate and printing speed, ensuring stable material deposition. (b) In contrast, multi-axis 3D printing with curved layers introduces varying layer heights across different regions, necessitating an *adaptive adjustment* of the local material deposition rate. To address this challenge, we propose a force-based method that dynamically regulates the printer head's moving speed while maintaining a constant extrusion rate, enabling adaptive deposition through a force-based closed-loop control (details presented in Sec. 3). (c) A comparative analysis of tensile strength on the Bracket models printed using different methods – geometry-based vs. force-based – demonstrates the effectiveness of our approach, with specimen weights provided for reference. The parameter α stands for adaptive deposition factor, which will be explained in detail in Sec. 3.2.

1. Introduction

Additive manufacturing (AM), commonly known as 3D printing, has garnered significant attention for its ability to fabricate complex geometries with high design flexibility [1–3]. Among various AM technologies, Fused Deposition Modeling (FDM) is widely adopted due to its low cost and operational simplicity, making planar 3D printing commercially viable [4]. However, as demand for customized manufacturing grows, the fixed-axis nature of planar printing imposes inherent constraints [5]. To address these limitations, multi-axis 3D printing has emerged as a promising alternative [6, 7]. By introducing additional degrees of freedom, multi-axis printing enables the reduction of support

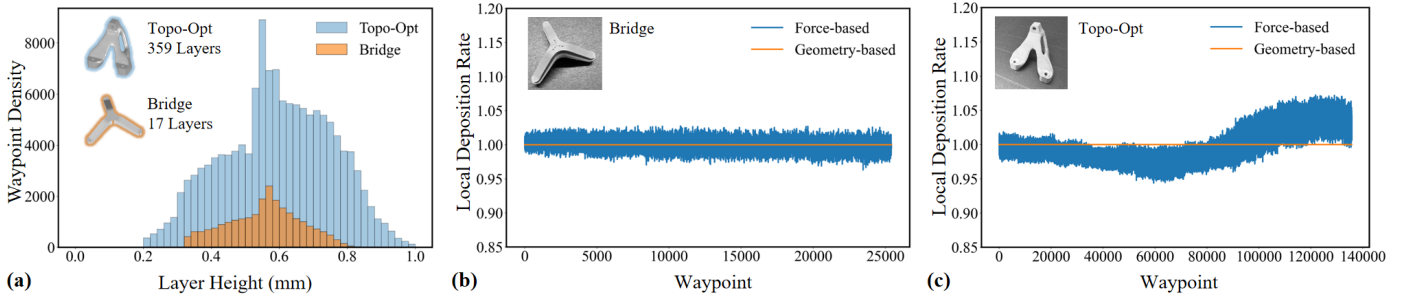


Figure 2: When curved layers are generated by following the principal stress orientations, large variations can be observed on layer thickness, as shown in (a). By studying the local material deposition rates obtained from our force-based method, it can be observed that larger ‘gaps’ need to be fixed in the later layers due to the accumulated voids. Two models are studied – (b) the Bridge model with 17 layers and (c) the Topo-Opt model with 359 layers. The geometry-based results shown here have their deposition ratio normalized according to the weights of force-based results.

structures [8], the improved surface quality [9], and, most notably, the alignment of printing layers with principal stress directions, significantly enhancing mechanical strength [6, 10, 11].

1.1. Problem definition

Despite its advantages, multi-axis 3D printing presents a fundamental challenge: achieving well-controlled material deposition over curved surfaces. Unlike planar printing, which benefits from uniform layer height and consistent deposition conditions, multi-axis printing must accommodate continuously varying surface curvatures and deposition angles. This inevitably leads to non-uniform layer thickness, making consistent material deposition unachievable in practice. The resulting variations can cause over- or under-extrusion, surface defects, poor inter-layer bonding, and internal voids that weaken the structural performance of printed parts [12]. These challenges are further complicated by unpredictable process errors, such as inaccurate extrusion control – caused by motion [13], the collapse of earlier layers, or hardware malfunctions. Such errors can accumulate over time, especially in geometrically complex regions. Since these uncertainties are difficult to predict or model accurately in advance, geometry-driven offline planning alone is often inadequate for ensuring reliable print quality and mechanical robustness in multi-axis additive manufacturing.

Figure 1 highlights both the advantages and challenges of multi-axis 3D printing with curved layers. Unlike conventional planar printing, where layer thickness remains uniform, curved-layer printing demands continuous adjustments to extrusion parameters to prevent porosity. The non-uniform layer dis-

tances (see Fig. 2(a)) affects both intra-layer and inter-layer bonding, making it difficult to achieve consistent material distribution. Existing toolpath generation strategies, such as contour, zigzag, and stress-aligned paths, struggle to ensure complete coverage in non-polygonal geometries since irregular filling areas often do not align precisely with the extrusion width [14].

Moreover, porosity-related errors accumulate over successive layers – i.e., larger voids form in later layers, particularly in prints with a high number of layers (see Fig. 2(c)). As a result, uncontrolled extrusion leads to insufficient filling density, reduced mechanical strength, and an increased risk of delamination and fracture [15–17]. This research aims to develop an adaptive deposition method to ensure sufficient filling density, ultimately enhancing the mechanical strength of 3D printed parts.

1.2. Our method

We propose a force-based sensing approach to monitor the filling density of previously printed layers in real time. By integrating a force sensor into the printer head, we obtain direct feedback on material deposition, enabling a closed-loop control strategy that dynamically adjusts the local deposition rate. This approach maintains a constant resistant force during printing, ensuring more uniform extrusion and reducing porosity. Rather than modifying the extrusion speed which can introduce delays and inconsistencies because of mechanical lag, stepper motor response limits and pressure changes in the melt cavity, we regulate the printer head’s motion while keeping the extrusion rate constant. This allows for rapid and precise adaptation to variations in layer height, particularly in regions with high curvature. Additionally, we develop a calibration method to determine the target resistant force, which is tailored to the specific material and hardware configuration. Experimental results demonstrate that our method significantly improves the mechanical strength of printed parts compared to purely geometry-based approaches (see Fig. 1(c)). Furthermore, our method can mitigate the effects of unstable extrusion caused by printer malfunctions, ensuring more consistent mechanical performance across different prints.

The technical contributions of our work are summarized as follows.

- We propose a force-based adaptive deposition method that can significantly reduce under-extrusion gaps in curved filament 3D printing, effectively enhancing the mechanical strength of printed models.
- We develop a calibration scheme to determine the target resistant force for adaptive deposition control, considering that the force parameter is tailored to specific materials and hardware configurations.

- We demonstrate that force-based adaptive deposition effectively compensates for density variations that arise from printer malfunctions, ensuring consistent print quality.

The effectiveness of our approach has been validated through tensile testing and *scanning electron microscope* (SEM) imaging on a variety of models fabricated with different materials.

2. Related Work

2.1. Quality control for 3D printing

To address the challenge of quality control, particularly porosity control, researchers have explored various strategies, including offline path planning, online error correction, and post-processing.

Offline path planning seeks to minimize void formation and enhance structural integrity by modifying the printing trajectory before printing begins [18, 19]. Ding et al. [20] proposed a path planning method based on geometric medial axis transformation (MAT) to generate gap-free paths for arbitrary geometries. Kuipers et al. [14] presented a framework which supports multiple schemes to generate toolpaths with adaptive width, by employing a function to decide the number of beads and their widths. Other works have explored hybrid toolpath strategies [21], pre-adjusted laser power for heat accumulation mitigation [22], and geometry-based extrusion compensation [11]. Additionally, defect elimination strategies such as vacuum assistance [23], tension and compaction [24], and energy-assisted techniques [25] have been explored for improving material properties on 3D prints.

Despite the effectiveness of pre-planning, deposition variability and process complexities make it difficult to fully eliminate print defects. This issue is amplified in curved printing, where robot dynamic and layer thickness change in optimal printing parameters increase the likelihood of defects. To address these challenges, in-situ monitoring and online correction techniques have been proposed [26]. Online correction methods allow real-time adjustments to deposition conditions, reducing dependency on predefined parameters and mitigating uncontrollable factors such as nozzle clogging. Various sensor-based monitoring methods have been explored, including acoustic emission [27], vibration analysis [28], and internal pressure sensing [29]. Zhang et al. [30] investigated the effect of printing pressure forces on the mechanical properties and void distribution of continuous carbon fiber reinforced polymer continuous carbon fiber reinforced polymer (CCFRP) composites, demonstrating that optimized layer thickness can generate a higher ironing force, minimizing void formation and improving

mechanical performance. Lu et al. [31] proposed a multi-sensing framework for process quality evaluation of CCFRP composites, integrating infrared, visual, force, and laser-displacement sensors to assess surface quality and fiber misalignment. However, their approach primarily focuses on post-process defect analysis and offline parameter optimization. Again, only planar-layer based printing has been studied. In summary, the existing approaches with in-situ monitoring have not been employed to reduce the porosity in filament based 3D printing by adaptively changing the local extrusion volume, especially for multi-axis 3D printing with curved layers.

Image-based techniques offer an intuitive and cost-effective approach for in-situ monitoring, with methods such as 3D imaging for layer contour extraction [32] and visual marker-based error tracking [33]. Depth camera-based model reconstruction [34] and image texture analysis for defect detection [35] have also been explored. However, these methods are highly sensitive to lighting conditions and surface characteristics, and real-time correction is often hindered by occlusions from the print head. To enhance robustness, learning-based approaches have been integrated into 3D printing monitoring and correction [36]. Supervised learning models have shown promise for defect classification [37, 38], while deep learning techniques have enabled defect compensation in fiber-reinforced polymers [39]. Despite these advancements, such methods depend on extensive manually labeled datasets, making them impractical for complex multi-axis printing. Although automatic labeling techniques such as [40] can be proposed, their applicability remains limited to planar printing and unsuitable for complex curved layer printing since the parameters need to be changed adaptively in curved printing.

Post-processing strategies, including heat treatment [41], ironing [42], and laser polishing [43], have been employed to enhance print quality. However, these methods can significantly extend manufacturing time and may alter the geometry of printed parts, potentially affecting their dimensional accuracy.

2.2. Force feedback for correction

Multi-axis additive manufacturing allows dynamic control of printing orientations, enabling advanced capabilities such as support-free fabrication [5], improved surface quality [44], and reinforcement of mechanical strength [10, 45]. However, existing curved slicing methods often sacrifice layer thickness uniformity to achieve these benefits, introducing a core challenge addressed in this work – accurate, spatially adaptive control of material deposition rates. Additionally, deposition errors in early layers tend to accumulate in later layers, which cannot be corrected by conventional offline, geometry-oriented plan-

ning. Unlike earlier systems with fixed, downward-facing printheads [5, 10], recent configurations permit changes in the printhead’s orientation relative to gravity, either to reduce calibration errors [11] or to improve kinematic performance [46, 47]. This added flexibility further increases differences between planned and actual layer heights. Existing in-situ monitoring and control techniques are typically designed for planar printing with fixed angles [40, 48], and thus fall short in addressing the complex, multi-factor challenges introduced by multi-axis printing with curved layers. Therefore, a new method is required for adaptive material deposition in multi-axis additive manufacturing to control porosity and achieve enhanced mechanical strength in the final print.

The use of force sensing for monitoring and control in 3D printing is a relatively recent advancement. Fischer et al. [49] proposed a compact approach to measure internal forces within the extruder, enabling adaptive parameter tuning for more uniform extrusion. Similarly, Coogan et al. [50] embedded pressure ports in the nozzle to measure melt pressure and monitor the printing process. However, these studies focused on simple planar scenarios. More recently, Guidetti et al. [48] introduced force-controlled printing for filament-based deposition, using a closed-loop system to regulate extrusion volume. Their results revealed a strong correlation between extrusion pressure and deposited line width, highlighting the potential of force feedback for adaptive deposition. However, their control strategy adjusts the extrusion motor speed, which often incurs significant response delays and assumes consistent layer height and planar toolpaths. In contrast, curved multi-axis printing involves continuously varying layer heights and surface geometries, demanding more reliable and low-latency control of material extrusion. Precise deposition in such cases can be more effectively achieved by modulating the printer head’s motion as the strategy employed in our method. Moreover, their approach does not account for gravity-induced effects or the complexities introduced by a rotated printer head, which are explicitly addressed in our method.

Force feedback systems address key limitations of traditional image-based monitoring by providing direct and real-time measurements of deposition conditions, reducing reliance on extensive datasets and complex calibration procedures. By integrating force feedback into curved 3D printing processes, we present a novel method to control density therefore optimize the mechanical strength of 3D printed parts.

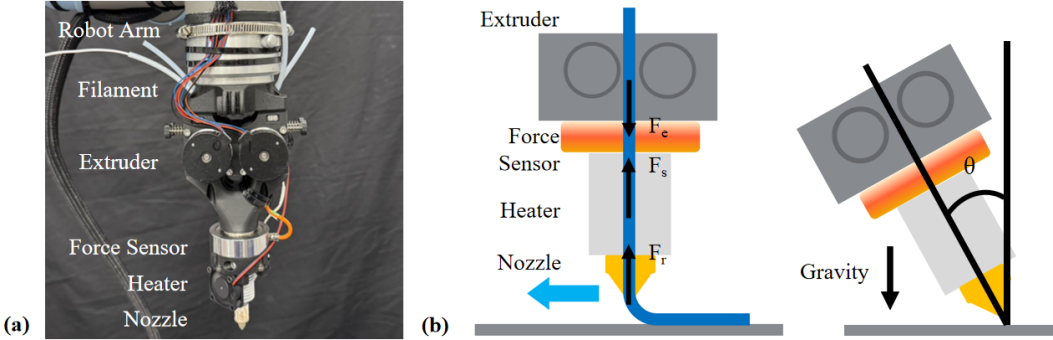


Figure 3: Illustration of our printer head equipped with a force sensor. (a) The printer head comprises a force sensor, a heating system, and four extruders capable of handling different materials. (b) During the printing process, the sensed force is influenced by the weight of the printer head, which varies with different printing angles θ .

3. Force-Based Adaptive Deposition

3.1. Sensor and resistant force

Our printer head design incorporates a convex circular force sensor (model RDF-K50 from RLD-sensor) to measure the resistant force on the cold end in real time during printing. The printer head consists of several components arranged from top to bottom: the filament feed tube, extruder, force sensor, heater with fan, and nozzle (see Fig. 3(a) for an illustration). To support multi-material printing, our design includes four extruders, with different filaments inserted into the same through-hole of the sensor at different times. The force sensor outputs an analog signal, which is converted into a standard voltage signal and then mapped to physical force through a transmitter, providing force feedback for the closed-loop control of adaptive deposition. The sensor offers a resolution of 0.001 N and a response speed of 2500 Hz. Having such a high response speed, the delay caused by signal transmission becomes negligible – considering that the printing speed of filament-based deposition is usually at around 3-4 mm/second.

The lab-made extruder based on HGX-Extruder Kit is driven by a motor, and the drive wheel connected to the motor is in contact with the filament. When the drive wheel rotates, the extrusion force F_e is applied to the filament. As illustrated in the left of Fig. 3(b), the extrusion force F_e is counteracted by the surface friction force F_s generated between the material and the nozzle wall and the printing resistance force F_r as $F_e = F_s + F_r$. However, these forces cannot be directly measured by the force sensor.

The force measured by the sensor includes both the extrusion force F_e and

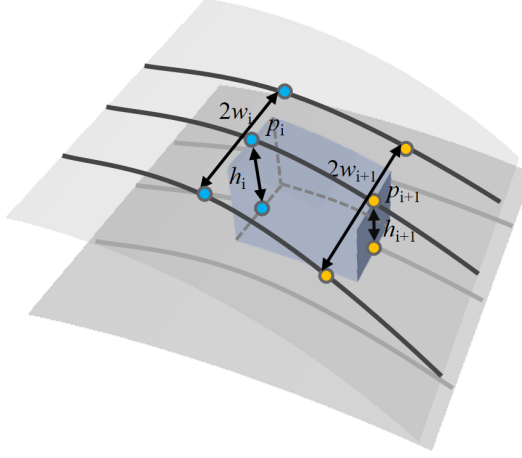


Figure 4: Illustration of how to estimate the required material extrusion volume based solely on geometric information.

the total weight F_g of the extruder and the heating module applied along the axial direction, which however is dependent to the tilting angle θ of the printer head as illustrated in the right of Fig. 3(b). That is

$$F_m = F_e + F_g \cos \theta = F_r + F_s + F_g \cos \theta, \quad (1)$$

where the values of F_g and F_r can be obtained by the force measurements taken in special cases. That is:

- No extrusion: When placing the printer head vertically (i.e., $\theta = 0$) and stopping extrusion, the gravity force F_g is measured by the force sensor.
- Extrusion in ‘free-load’: While extruding materials in a ‘free-load’ way – i.e., keeping nozzle tip away from the working surface and $\theta = 0$, the measured force is $F_0 = F_s + F_g$ with $F_r = 0$.

In summary, the resistant force F_r can be obtained from the online measured force F_m by

$$F_r = F_m - F_0 + (1 - \cos \theta) F_g. \quad (2)$$

3.2. Force-based control

In our approach, the local material deposition rate is controlled by precisely adjusting the printer head’s moving speed, which can be executed without delay. Given w_i and w_{i+1} as the average distances from waypoints \mathbf{p}_i and \mathbf{p}_{i+1}

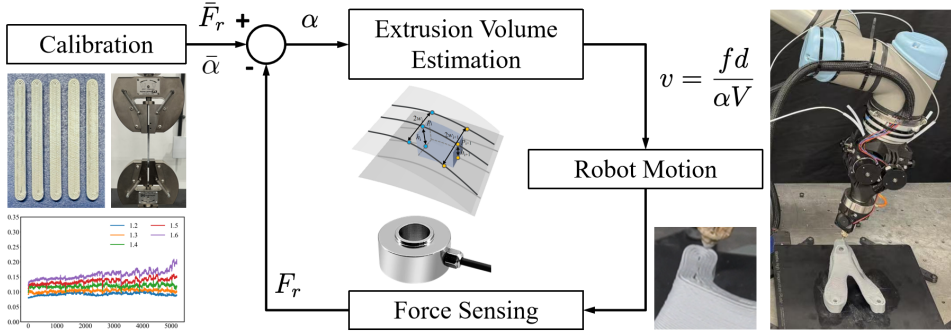


Figure 5: Schematic of the force-based adaptive deposition control pipeline. The system calibrates the target resistance force \bar{F}_r using tensile bar specimens, paired with a standard amplification factor $\bar{\alpha}$. During adaptive control, the measured force F_r is continuously compared with \bar{F}_r to dynamically adjust the amplification factor α , which modulates the robot's motion speed v and, consequently, the local material deposition volume. This closed-loop control ensures optimized print density and reduced porosity.

to the adjacent toolpath on the same curved layer, and h_i and h_{i+1} as the layer thickness at these points (see Fig. 4 for an illustration), the required material extrusion volume V (mm^3) can be estimated as

$$V = \frac{d}{4}(w_i + w_{i+1})(h_i + h_{i+1}), \quad (3)$$

where d (mm) is the distance between p_i to p_{i+1} . The moving speed v ($\text{mm}/\text{min.}$) of the printer head's nozzle tip is then determined by

$$v = \frac{fd}{\alpha V}, \quad (4)$$

where f ($\text{mm}^3/\text{min.}$) is the extruder feed rate, and α is an amplification factor controlling the level of over- or under-extrusion. Specifically, setting $\alpha < 1.0$ results in under-extrusion and increased porosity, while increasing α slows the printer head's motion, allowing more material to accumulate locally and increasing density. In order to avoid the instability and safety problems of the robot arm caused by the excessively fast terminal motion speed when the curvature changes greatly, we limit the terminal motion speed to [1, 6] (mm/s). Note that, after using Eq.(4) to determine the new tip velocity v , we update the time variable t_{i+1} by

$$t_{i+1} = t_i + \frac{\|\mathbf{p}_i \mathbf{p}_{i+1}\|}{v} \quad (5)$$

while keeping the positions and orientations at waypoints \mathbf{p}_i and \mathbf{p}_{i+1} unchanged. The waypoints of toolpath are adaptively generated with reference to the curvature – i.e., denser waypoints are generated in regions with higher curvature. The updated motion of robotic arm can be easily determined by the computation of inverse kinematics.

The adaptive deposition factor α is determined based on the sensed resistance force F_r . When using different materials or printer heads, a calibration process¹ is first conducted to obtain a target reference force \bar{F}_r along with a standard amplification factor $\bar{\alpha}$. During adaptive deposition, α is dynamically adjusted at each waypoint according to

$$\alpha = \bar{\alpha} \left(\frac{\bar{F}_r}{F_r} \right)^k, \quad (6)$$

where $k \in (0, 1)$ controls the sensitivity of the adjustment. A smaller k results in a more gradual response, ensuring smooth deposition across varying layer heights and preventing abrupt material flow changes. In our implementation, we choose $k = 0.5$ by experiments.

This method for adjusting α (therefore the robot motion speed by Eq. (4)) ensures that when the sensed resistance force F_r is lower than the target force \bar{F}_r – indicating low density – more material is deposited to compensate. Conversely, if F_r exceeds \bar{F}_r , signifying over-extrusion, the material deposition rate is reduced by decreasing α . These adjustments are effectively regulated by Eq. (6), enabling real-time control of deposition density. The control pipeline is shown in Figure 5.

While adaptively changing the moving speed v can alter the path width of the printout when no neighboring paths exist, this is not an issue for interior toolpaths of a surface patch, where adjacent paths are always present. In practice, we therefore begin by printing the boundary paths using a constant standard amplification factor α . The force-based adaptive printing strategy introduced in this paper is then applied to the interior toolpaths. It is also worth noting that layer thickness is determined entirely by the nozzle tip positions of neighboring curved layers planned by slicers, and thus remains unaffected by the motion speed.

The effectiveness of our method is demonstrated by the experimental results shown in Fig. 6. For the Bracket model, we initially employed a purely geometry-based approach (i.e., constantly setting $\alpha = 1.0$) to print the first 20

¹Details of this calibration process are provided in Sec. 3.3.

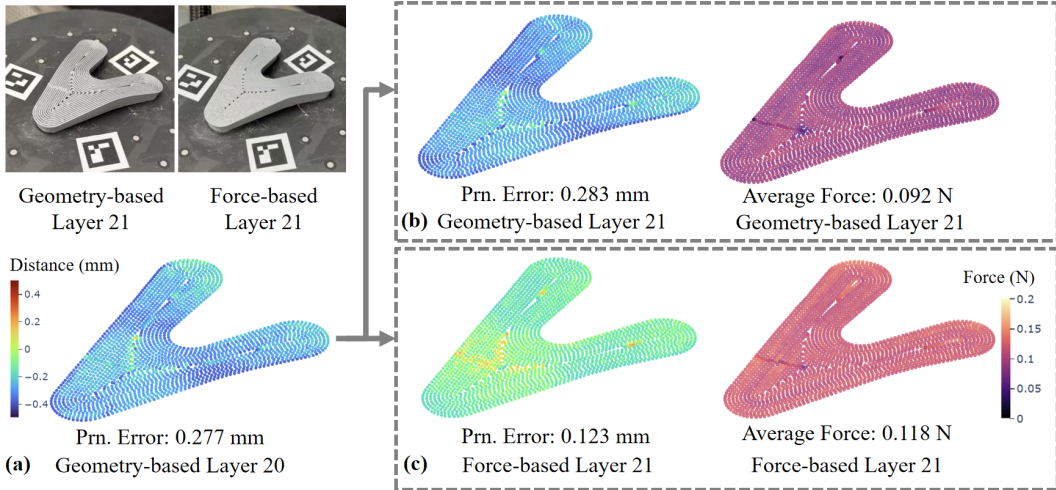


Figure 6: Geometric errors of a partially printed model (after 20 layers) are measured using a 3D scanner with markers for rigid registration and visualized through a color map (a). The next layer is then printed using both a purely geometry-based deposition approach (b) and the proposed force-based adaptive deposition (c). Geometric errors and sensed forces at all waypoints are represented using color maps, with the target reference force set to 0.12N.

layers. As voids accumulated, significant structural collapse was observed, as evident in the 3D-scanned result in Fig. 6(a). When the force-based method was applied for the subsequent layer, the geometric error was effectively reduced, as shown in Fig. 6(c), in contrast to the geometry-based approach in Fig. 6(b).

3.3. Target reference force

This subsection presents the calibration method for determining the target reference force \bar{F}_r and the standard amplification factor $\bar{\alpha}$ together, both of which are material- and machine-dependent. To illustrate the process, we use two example materials shown in Fig. 7: *Polylactic Acid* (PLA) and *Polylactic Acid with Carbon Fiber* (PLA-CF).

For each material, several tensile bar specimens are printed using different amplification factors α while recording the corresponding sensed forces. These specimens then undergo tensile testing to determine their respective failure loads as the breaking forces of specimens. The first derivative of the failure load curve is analyzed to identify the turning point – where increasing the local extrusion rate no longer significantly enhances the failure load. Beyond this point, further extrusion leads to over-extrusion and associated defects. The amplification factor α and the average sensed force at this turning point are

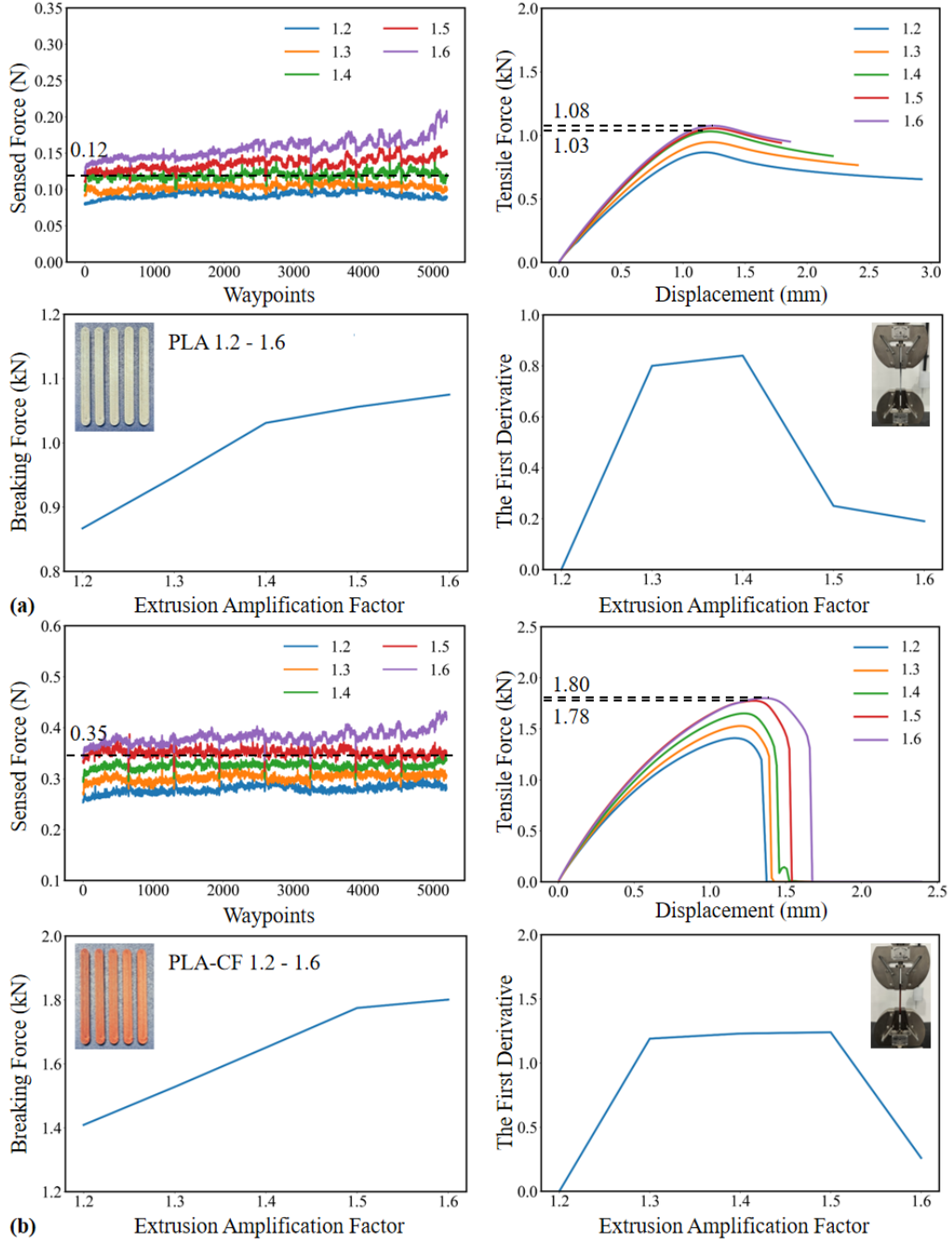


Figure 7: The calibration process was conducted for two different materials: (a) PLA and (b) PLA-CF. For each material, specimens were printed using various amplification factors (i.e., $\alpha = 1.2, 1.3, \dots, 1.6$). Tensile tests were then performed to obtain failure loads from the force-displacement curves, and the first derivatives were calculated to determine the values of \bar{F}_r and $\bar{\alpha}$ at the turning point.

selected as the calibrated values: $\bar{\alpha}$ and \bar{F}_r .

To verify repeatability and reliability, the calibration process is conducted multiple times for each material. As shown in Fig. 7, the calibrated values are $\bar{\alpha} = 1.4$, $\bar{F}_r = 0.12$ N for PLA and $\bar{\alpha} = 1.5$, $\bar{F}_r = 0.35$ N for PLA-CF. It is worth noting that such a calibration process is a standard practice across all filament-based 3D printing systems. In particular, system-specific parameters – such as $\bar{\alpha}$ and \bar{F}_r in our method – must be recalibrated whenever the printer nozzle is changed or a new, previously untested material is used.

4. Results and Discussion

We have implemented the proposed control method in Python and the physical fabrications have been conducted on a robot-assisted multi-axis 3D printing system to verify the effectiveness of our method. Details are introduced below and a supplementary video can be found at: https://youtu.be/i_Gpd3_gRxA.

4.1. Hardware system

The robot-assisted additive manufacturing system employed in our experiments is as illustrated in Fig. 8. The printer head is mounted on the end-effector of a UR5e robot arm with 6 degrees-of-freedom for curved 3D printing. Extruder control is managed by a Duet 3D board dedicated to 3D printing. Synchronization between the robot arm and the extrusion signals is achieved through a laptop by Python code, which simultaneously sends movement commands to the robot arm control box and extrusion signals to the Duet 3D board via a router. The transmitter used in our system performs internal calibration and conversion from analog voltage to physical force. Note that the adaptive deposition method and the sensing hardware introduced below can be easily extended to 3D printing systems with other configurations of motion stages (e.g., the 5-axis systems discussed in [10, 13]). Tensile / compression tests are all conducted on an INSTRON tensile machine 5960.

4.2. Physical validation

We have physically fabricated a few models and conducted the tensile tests to demonstrate the enhancement of mechanical strength that can be achieved by our adaptive deposition method.

The first example is the Bracket model, as shown in Fig. 1(c), which is fabricated using both planar and curved layers. To ensure a fair comparison, we first print the model using our force-based method. The weight of the resulting model is then used to determine a constant amplification factor, α ,

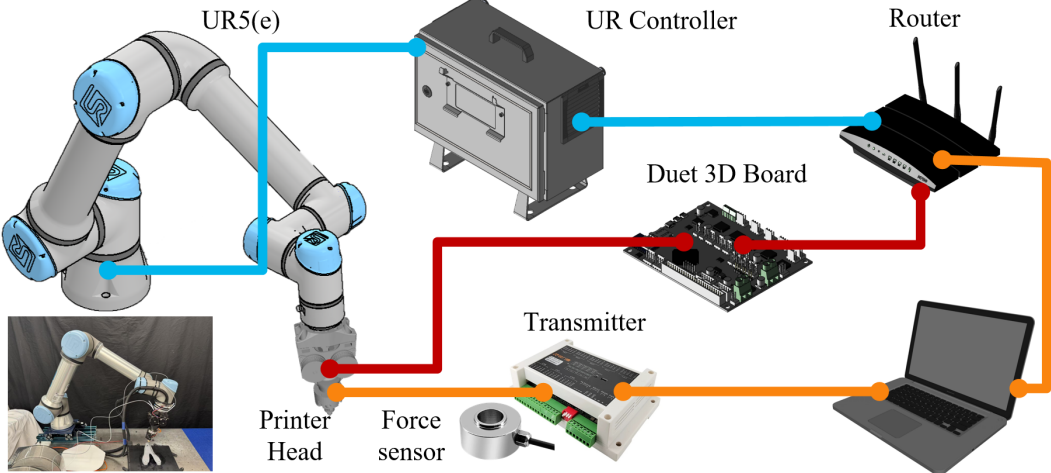


Figure 8: Illustration of our hardware system for multi-axis 3D printing – the control diagram of a UR5e robot arm and a print head working in a synchronized way. Different from the hardware used in our earlier work (e.g., [51]), a force sensor is integrated with the extruder controller on the printer head.

which in turn defines the moving speed v via Eq. (4). Based on this approach, we obtain $\alpha = 1.35$ and $\alpha = 1.30$ for pure geometry-based printing. Tensile test results reveal that the failure load of specimens printed using our method is significantly higher than those printed with the geometry-based approach, even after increasing their weight – and consequently the extrusion ratio – by 35% and 30%, respectively. This example is also employed to demonstrate the strengthen that can be achieved by multi-axis additive manufacturing.

The second example is the Bridge model, as shown in Fig. 9. Our force-based method is compared with the results obtained from geometry-based methods with and without extrusion amplification. The force-displacement curves obtained from the compression tests indicate that the force-based method and the curved slicing strategy can still significantly enhance mechanical strength compared to geometry-based approaches even after normalizing the weights – i.e., using $\alpha = 1.38$ (curved) and $\alpha = 1.35$ (planar) respectively. In short, the force-based printing by curved layers can achieve 1) 42.7% larger failure load than the geometry-base planar printing and 2) 11.9% larger failure load than the geometry-based curve printing – both for specimens having the similar weights.

We further validated our results using scanning electron microscopy (SEM) on the Bridge model printed by curved layers, as shown in Fig. 10. The images of cross-sections at different scales reveal that the geometry-based print exhibits

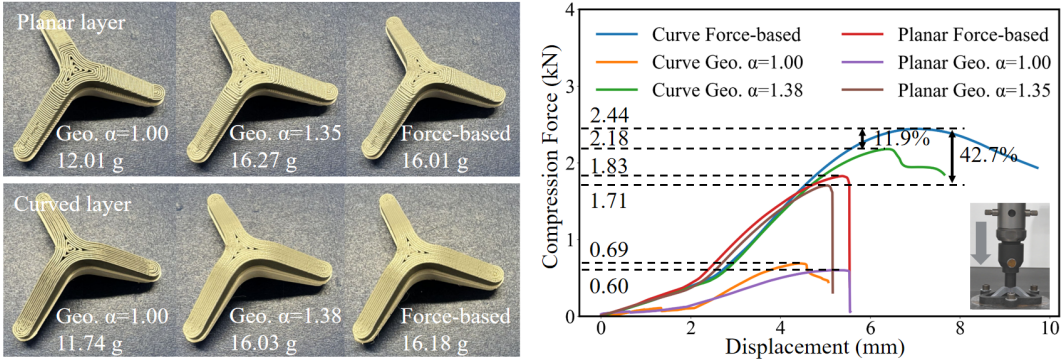


Figure 9: This figure compares the outcomes of planar and curved layer-based printing strategies using geometry-based (Geo.) and force-based methods on the Bridge model.

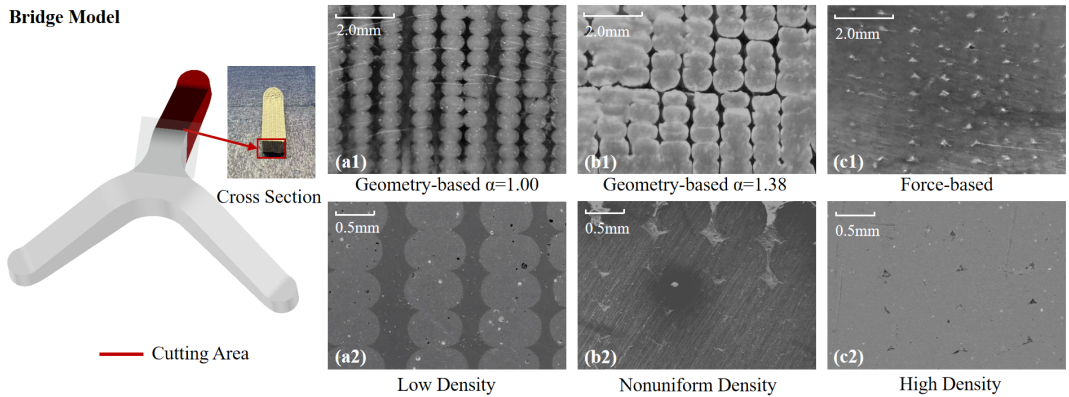


Figure 10: SEM images of cross-sections comparing geometry-based printing with different adaptive deposition factor $\alpha = 1.00$ (a1-a2) and $\alpha = 1.38$ (b1-b2) vs. our force-based printing (c1-c2).

either high porosity (when $\alpha = 1.00$) or nonuniform density (with $\alpha = 1.38$ but still have large gaps between filaments), whereas the force-based print shows significantly reduced voids with significant higher density. This finding directly correlates with the enhanced mechanical strength observed in specimens fabricated using our force-based method. Note that the geometry-based approach applied here has considered the local geometric shape, the layer thickness variation and also the distance variation between neighboring toolpaths. Also, the waypoints on toolpaths are generated by adaptive sampling according to the curvature of toolpaths.

An interesting phenomena we observed during the physical experiments is that the errors in the earlier layers will be accumulated to generate larger errors in the later layers. Therefore, the models with a large number of layers will have

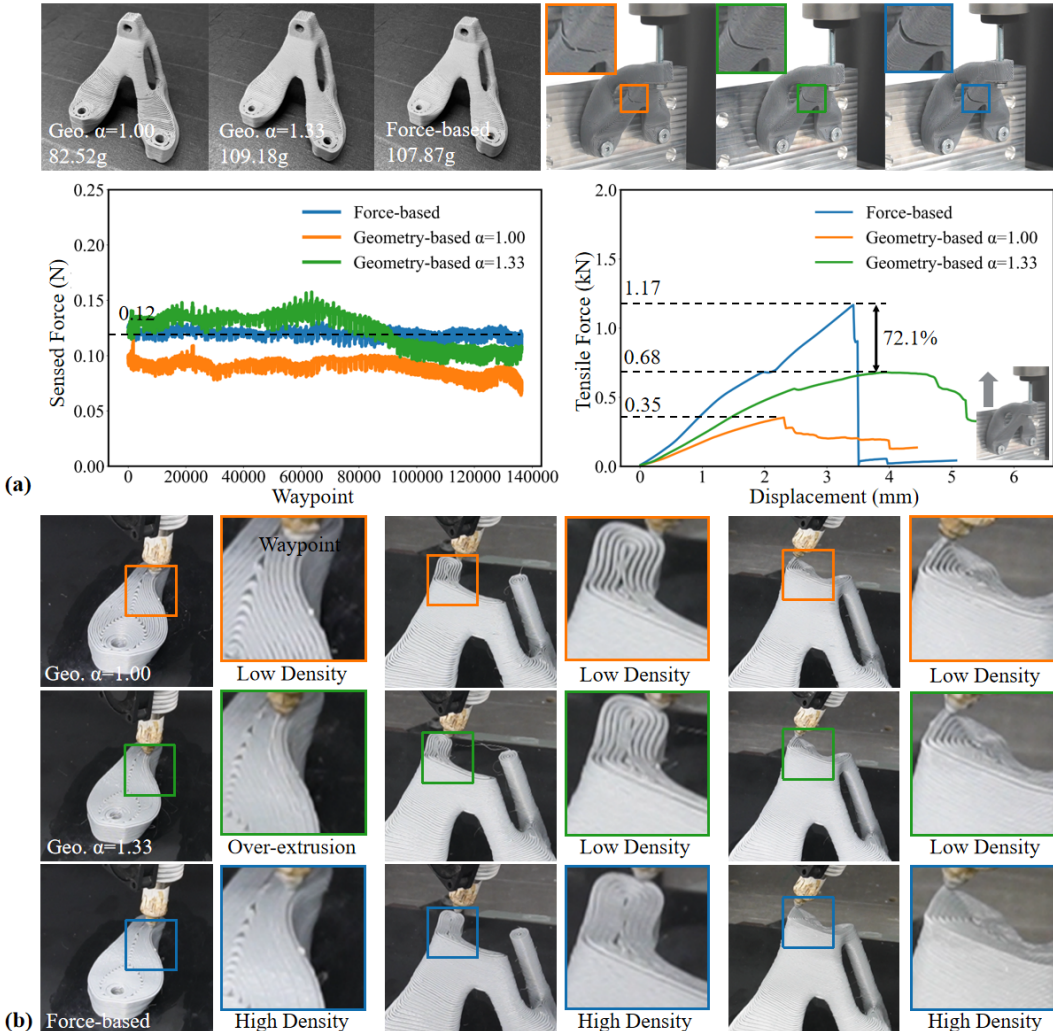


Figure 11: Demonstration of our force-based adaptive deposition on a Topo-Opt model with 359 curved layers. (a) Tensile test results and the sensed forces during printing processes, showing that our force-based adaptive deposition achieves a more stable resistance force around the calibrated target value of 0.12N. On the contrast, the geometry-based method exhibits greater fluctuations on the resistant forces – i.e., inconsistent local densities, leading to poor mechanical strength. (b) Photos captured during the printing process, highlighting uncontrolled voids (leading to low density) and over-extrusion in geometry-based printing results.

more problems in general. We apply our force-based adaptive deposition on two such models – i.e., a Topo-Opt model (see Fig. 11) and a Bunny-Head model (see Fig. 12). For the example of Topo-Opt model, both the geometry-based

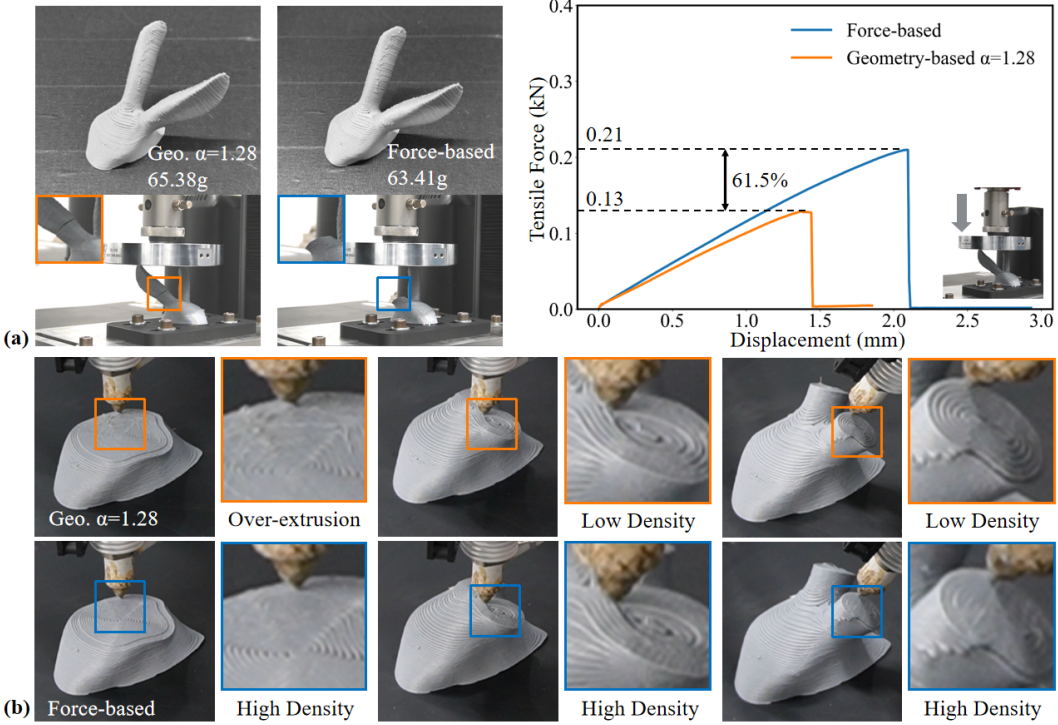


Figure 12: The comparison of geometry-based vs. force-based prints on the Bunney-Head model with 251 curved layers. (a) The results of tensile tests. (b) The photos of printing processes.

and the amplified geometry specimens are printed, where the amplified result is again normalized (with $\alpha = 1.33$) according to the weight of the force-based result. Again, for the geometry-based result of the Bunny-Head model, the extrusion is normalized (with $\alpha = 1.28$) according to the weight of force-based result. In these comparison, our force-based method can effectively improve the failure loads by 72.1% and 61.5% respectively.

4.3. Different materials

All examples presented above were printed using PLA filaments at a temperature of 210°C, with an extruder feed rate of 35.0 mm³/min.. We conduct the other test to verify the effectiveness of our approach on different materials – the PLA and the PLA-CF. Both are based on the target reference force and the standard amplification factor as obtained in Sec. 3.3. The printing temperature for PLA-CF is set as 230°C.

The tests were conducted on the Bracket model, as shown in Fig. 13. For the PLA results, in addition to those presented in Fig. 1, we included a purely

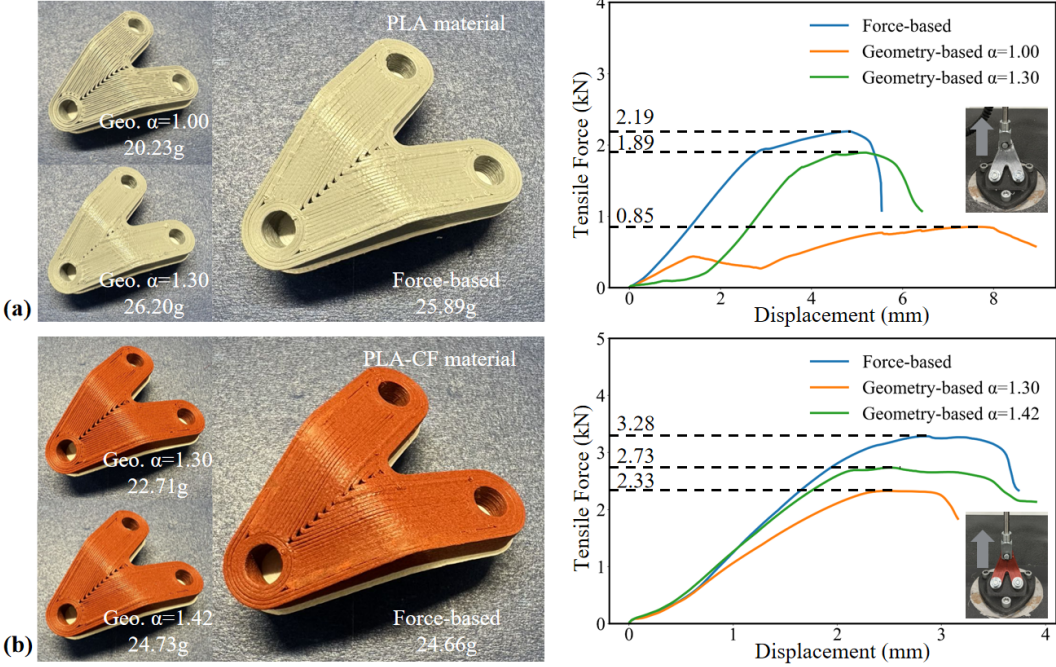


Figure 13: Comparison of 3D printed parts using different materials – (a) PLA and (b) PLA-CF. The Bracket model is also printed by different extrusion-control strategies.

geometry-based print ($\alpha = 1.00$), which is significantly lighter than the one printed with an extrusion rate normalized to match the weight of the force-based result ($\alpha = 1.30$). When using PLA-CF with the same constant amplification factor ($\alpha = 1.30$), the printed model was lighter but exhibited greater strength compared to the PLA version. Similarly, we fabricated the PLA-CF Bracket using both the force-based and the geometry-based method, with the latter normalized by weight ($\alpha = 1.42$). The failure load of the specimen printed using our force-based method was 20.2% higher than that of the geometry-based print with a similar weight.

4.4. Imperfection compensation

During the printing process, uncontrolled imperfections can arise due to random hardware malfunctions, such as nozzle blockages or filament depletion. These issues often lead to defects in the printed structure, significantly compromising mechanical strength. Conventional offline planning methods are unable to address such problems, whereas our force-based approach can effectively compensate for these errors in real time.

To demonstrate this capability, we intentionally omitted a portion of the

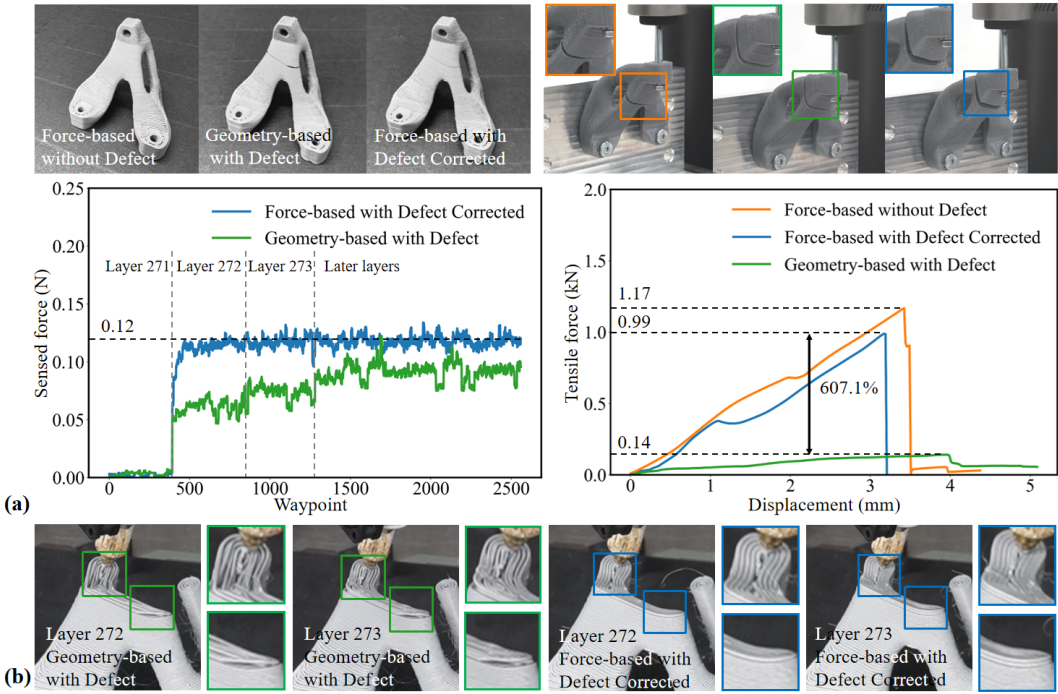


Figure 14: An experimental test taken on the Topo-Opt model demonstrating the capability of our force-based method to compensate for imperfections caused by a missing portion of the 271st layer. (a) The sensed resistant forces in relevant layers and the tensile test results. (b) Comparison of material deposition between the force-based and geometry-based methods.

271st layer in the Topo-Opt model (Fig. 14) to simulate imperfections caused by hardware malfunctions. As shown in Fig. 14, our force-based method adaptively increases local material deposition in the 272nd layer and the 273rd layer to compensate for the missing section, effectively filling the gap. In contrast, the geometry-based method lacks such adaptability. These differences are also reflected in the sensed forces – i.e., our adaptive deposition method can effectively raise the resistant forces back to the required level as 0.12N, which is failed to achieve by the geometry-based method.

Tensile test results indicate that when both methods experience the same imperfection, our force-based approach improves mechanical strength by 607.1% compared to the geometry-based method. Moreover, despite the introduced imperfection, the failure load of our force-based result is only 15.4% lower than that of the perfectly printed force-based adaptive deposition, demonstrating the robustness of our approach.

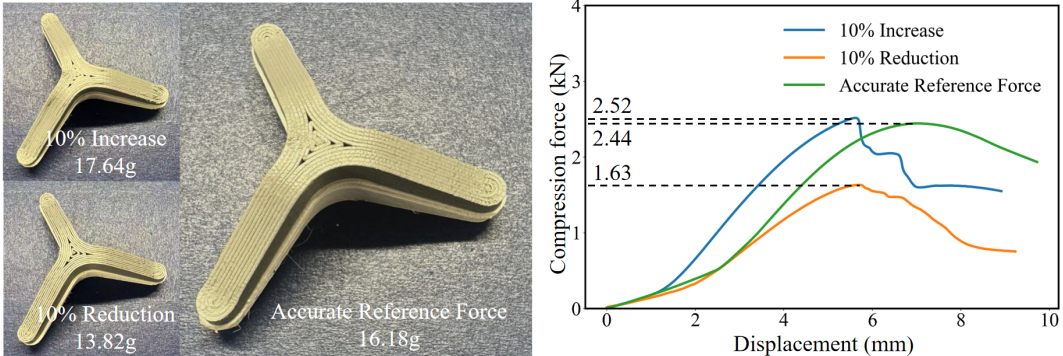


Figure 15: The study of inaccurate calibration’s influence – i.e., with the target reference force increased and reduced by 10%. This test also demonstrates the performance improvement limit when further increasing the target reference force.

4.5. Inaccurate calibration

Lastly, we investigate the impact of inaccurate calibration on the quality of printed results. Specifically, we fabricated the PLA Bridge model using a target reference force \bar{F}_r that was intentionally increased or decreased by 10% while keeping the value of $\bar{\alpha} = 1.4$ unchanged. Compression tests were then conducted on these specimens.

The results, presented in Fig. 15, reveal the following:

- An overestimated target reference force leads to over-extrusion, resulting in a heavier printed part with a slight improvement in mechanical strength.
- An underestimated target reference force causes severe under-extrusion, leading to voids and gaps throughout the model, significantly compromising its structural integrity.

These findings highlight the importance of precise calibration of both the standard amplification factor and the target reference force to prevent under-extrusion and ensure optimal print quality.

4.6. Limitation and future work

In our method, adaptive deposition is achieved by adjusting the motion speed of the printhead, rather than controlling the extruder’s feedrate. This strategy effectively mitigates several issues associated with extruder dynamics—such as lag and fluctuations in melt chamber pressure. However, it may also introduce other challenges, such as vibrations in the robotic arm. In future

work, we plan to incorporate offline kinematic optimization techniques [46] into the inverse kinematics computation to address these issues. Additional flexibility can be introduced by allowing controlled variations in extruder feedrate.

We adopt a simple proportional-only feedback law (i.e., Eq. (6)) in our closed-loop control, which performs well in practice for relatively slow printing motions and materials such as PLA and PLA-CF that exhibit low mechanical non-linearity. Our preliminary trials with more advanced strategies, such as a Proportional-Integral-Derivative (PID) controller, showed no significant performance improvement for filament-based deposition of PLA. It remains an open question whether PID control may offer greater benefits when printing materials with lower viscosity at higher speeds, which we plan to explore in future work.

In our implementation, the control algorithm runs on a laptop using Python to coordinate the entire printing process. As illustrated in Fig. 8, force sensor signals are processed by a transmitter and sent to the laptop, where the required velocity adjustments are computed. The updated motion commands are then relayed to the UR5e robot controller, while extrusion commands are sent to the Duet 3D board via a router. Although signal transmission introduces minor delays, experimental measurements show that the end-to-end delay for force data acquisition and processing is less than 1ms. At a maximum print speed of 6 mm/s (average 3–4mm/s), this corresponds to a spatial error of approximately 0.006mm – well below the nozzle diameter and the resolution of the printing system. Therefore, while such delays exist, their impact on the stability and accuracy of our force-based adaptive deposition strategy is trivial and can be neglected.

5. Conclusion

This paper presents a force-based closed-loop control method for adaptive deposition in multi-axis additive manufacturing. By directly regulating the deposition process through in-situ force feedback, our method significantly reduces internal porosity in filament-based printing and leads to substantial improvements in mechanical strength – even when using a simple proportional control law. Unlike prior geometry-aware or over-extrusion strategies that rely solely on offline planning, our approach closes the loop by dynamically adjusting motion speed in response to real-time resistance force, making it inherently robust to material flow variation and system imperfections. To enable this control paradigm, we have introduced a practical calibration scheme to determine the target resistance force, tailored to the material and hardware configuration.

The target force need only be determined once per material, offering a reusable and material-dependent control baseline that avoids tedious per-model tuning.

Through extensive experiments on diverse geometries and two materials, our method has demonstrated a consistent ability to compensate for extrusion irregularities – such as those caused by nozzle clogging or under-extrusion – by accumulating material in low-density regions during the printing process. This level of robustness is difficult to achieve through open-loop methods. Several scientific insights can be concluded:

- Porosity in curved multi-axis deposition stems from multiple factors – such as surface curvature, varying layer thickness, and unstable extrusion – none of which can be fully resolved through offline planning alone;
- A strong link is established between the measured resistance force, internal porosity, and mechanical performance, enabling a systematic shift from empirical model-dependent tuning to repeatable, material-dependent calibration;
- The proposed method automatically compensates for under-extrusion caused by malfunctions, such as partial nozzle jams, by adjusting deposition speed in real-time – i.e., closing the loop without the need for explicit defect detection.

In summary, this work demonstrates that even a simple force-based closed-loop controller can significantly enhance the mechanical performance of multi-axis 3D-printed structures. It highlights the importance of moving beyond open-loop geometric planning toward real-time, feedback-driven strategies in advanced additive manufacturing.

Declaration of competing interest

The authors declare that they have no known competing financial interests or personal relationships that could have appeared to influence the work reported in this paper.

Data availability

Dataset of models and tests conducted in this paper can be accessed at the following link: <https://github.com/yuminghuang1995/ForceBasedDeposition>.

Acknowledgments

The project is partially supported by the chair professorship fund at the University of Manchester and the UK Engineering and Physical Sciences Research Council (EPSRC) Fellowship Grant (Ref.#: EP/X032213/1).

References

- [1] W. Gao, Y. Zhang, D. Ramanujan, K. Ramani, Y. Chen, C. B. Williams, C. C. Wang, Y. C. Shin, S. Zhang, P. D. Zavattieri, The status, challenges, and future of additive manufacturing in engineering, *Computer-aided design* 69 (2015) 65–89.
- [2] F. P. Melchels, M. A. Domingos, T. J. Klein, J. Malda, P. J. Bartolo, D. W. Hutmacher, Additive manufacturing of tissues and organs, *Progress in polymer science* 37 (8) (2012) 1079–1104.
- [3] T. D. Ngo, A. Kashani, G. Imbalzano, K. T. Nguyen, D. Hui, Additive manufacturing (3d printing): A review of materials, methods, applications and challenges, *Composites Part B: Engineering* 143 (2018) 172–196.
- [4] X. Zhang, W. Fan, T. Liu, Fused deposition modeling 3d printing of polyamide-based composites and its applications, *Composites Communications* 21 (2020) 100413.
- [5] C. Dai, C. C. Wang, C. Wu, S. Lefebvre, G. Fang, Y.-J. Liu, Support-free volume printing by multi-axis motion, *ACM Transactions on Graphics (TOG)* 37 (4) (2018) 1–14.
- [6] T. Liu, T. Zhang, Y. Chen, Y. Huang, C. C. Wang, Neural slicer for multi-axis 3d printing, *ACM Transactions on Graphics (TOG)* 43 (4) (2024) 1–15.
- [7] Y. Yao, L. Cheng, Z. Li, A comparative review of multi-axis 3d printing, *Journal of Manufacturing Processes* 120 (2024) 1002–1022.
- [8] C. Wu, C. Dai, G. Fang, Y.-J. Liu, C. C. Wang, General support-effective decomposition for multi-directional 3-d printing, *IEEE Transactions on Automation Science and Engineering* 17 (2) (2019) 599–610.
- [9] D. Ahlers, F. Wasserfall, N. Hendrich, J. Zhang, 3d printing of nonplanar layers for smooth surface generation, in: 2019 IEEE 15th international

conference on automation science and engineering (CASE), IEEE, 2019, pp. 1737–1743.

- [10] G. Fang, T. Zhang, S. Zhong, X. Chen, Z. Zhong, C. C. Wang, Reinforced fdm: Multi-axis filament alignment with controlled anisotropic strength, *ACM Transactions on Graphics (TOG)* 39 (6) (2020) 1–15.
- [11] T. Zhang, G. Fang, Y. Huang, N. Dutta, S. Lefebvre, Z. M. Kilic, C. C. Wang, S3-slicer: A general slicing framework for multi-axis 3d printing, *ACM Transactions on Graphics (TOG)* 41 (6) (2022) 1–15.
- [12] X. Sun, M. Mazur, C.-T. Cheng, A review of void reduction strategies in material extrusion-based additive manufacturing, *Additive Manufacturing* 67 (2023) 103463.
- [13] T. Zhang, X. Chen, G. Fang, Y. Tian, C. C. Wang, Singularity-aware motion planning for multi-axis additive manufacturing, *IEEE Robotics and Automation Letters* 6 (4) (2021) 6172–6179.
- [14] T. Kuipers, E. L. Doubrovski, J. Wu, C. C. Wang, A framework for adaptive width control of dense contour-parallel toolpaths in fused deposition modeling, *Computer-Aided Design* 128 (2020) 102907.
- [15] X. Tian, T. Liu, C. Yang, Q. Wang, D. Li, Interface and performance of 3d printed continuous carbon fiber reinforced pla composites, *Composites Part A: Applied Science and Manufacturing* 88 (2016) 198–205.
- [16] L. Villalpando, H. Eiliat, R. J. Urbanic, An optimization approach for components built by fused deposition modeling with parametric internal structures, *Procedia Cirp* 17 (2014) 800–805.
- [17] C. W. Ziemian, R. D. Ziemian, K. V. Haile, Characterization of stiffness degradation caused by fatigue damage of additive manufactured parts, *Materials & Design* 109 (2016) 209–218.
- [18] Y. Huang, G. Fang, T. Zhang, C. C. Wang, Turning-angle optimized printing path of continuous carbon fiber for cellular structures, *Additive Manufacturing* 68 (2023) 103501.
- [19] Y. Huang, Y. Guo, R. Su, X. Han, J. Ding, T. Zhang, T. Liu, W. Wang, G. Fang, X. Song, et al., Learning based toolpath planner on diverse graphs for 3d printing, *ACM Transactions on Graphics (TOG)* 43 (6) (2024) 1–16.

- [20] D. Ding, Z. Pan, D. Cuiuri, H. Li, A practical path planning methodology for wire and arc additive manufacturing of thin-walled structures, *Robotics and Computer-Integrated Manufacturing* 34 (2015) 8–19.
- [21] Z. Wu, X. Sun, W. Dong, H. Wang, An interlayer interleaved hybrid path to optimize performance of material extrusion additive manufacturing, *Journal of Building Engineering* (2024) 111586.
- [22] H. Yeung, B. Lane, J. Fox, Part geometry and conduction-based laser power control for powder bed fusion additive manufacturing, *Additive manufacturing* 30 (2019) 100844.
- [23] B. B. Vatandaş, A. Uşun, R. Gümrük, Mechanical performances of continuous carbon fiber reinforced peek (polyether ether ketone) composites printed in a vacuum environment, *Journal of Manufacturing Processes* 120 (2024) 579–594.
- [24] N. Ichihara, M. Ueda, K. Kajiwara, A. Le Duigou, M. Castro, 3D printing with tension and compaction: prevention of fiber waviness in 3d-printed continuous carbon fiber-reinforced thermoplastics, *Advanced Composite Materials* 33 (3) (2024) 377–387.
- [25] R. Zhang, L. Yu, K. Chen, P. Xue, M. Jia, Z. Hua, Amelioration of interfacial properties for cgf/pa6 composites fabricated by ultrasound-assisted fdm 3d printing, *Composites Communications* 39 (2023) 101551.
- [26] Y. Fu, A. Downey, L. Yuan, A. Pratt, Y. Balogun, In situ monitoring for fused filament fabrication process: A review, *Additive Manufacturing* 38 (2021) 101749.
- [27] H. Wu, Y. Wang, Z. Yu, In situ monitoring of fdm machine condition via acoustic emission, *The International Journal of Advanced Manufacturing Technology* 84 (2016) 1483–1495.
- [28] Y. Tlegennov, W. F. Lu, G. S. Hong, A dynamic model for current-based nozzle condition monitoring in fused deposition modelling, *Progress in Additive Manufacturing* 4 (2019) 211–223.
- [29] C. Kim, D. Espalin, A. Cuaron, M. A. Perez, E. MacDonald, R. B. Wicker, A study to detect a material deposition status in fused deposition modeling technology, in: 2015 IEEE International Conference on Advanced Intelligent Mechatronics (AIM), IEEE, 2015, pp. 779–783.

- [30] Z. Zhang, Y. Long, Z. Yang, K. Fu, Y. Li, An investigation into printing pressure of 3d printed continuous carbon fiber reinforced composites, *Composites Part A: Applied Science and Manufacturing* 162 (2022) 107162.
- [31] L. Lu, S. Yuan, X. Yao, Y. Li, J. Zhu, W. Zhang, In-situ process evaluation for continuous fiber composite additive manufacturing using multisensing and correlation analysis, *Additive Manufacturing* 74 (2023) 103721.
- [32] Y. Cheng, M. A. Jafari, Vision-based online process control in manufacturing applications, *IEEE Transactions on Automation Science and Engineering* 5 (1) (2008) 140–153.
- [33] F. Baumann, D. Roller, Vision based error detection for 3d printing processes, in: *MATEC web of conferences*, Vol. 59, EDP Sciences, 2016, p. 06003.
- [34] S. Y. Chew, E. Asadi, A. Vargas-Uscategui, P. King, S. Gautam, A. Bab-Hadiashar, I. Cole, In-process 4d reconstruction in robotic additive manufacturing, *Robotics and Computer-Integrated Manufacturing* 89 (2024) 102784.
- [35] C. Liu, A. C. C. Law, D. Roberson, Z. J. Kong, Image analysis-based closed loop quality control for additive manufacturing with fused filament fabrication, *Journal of Manufacturing Systems* 51 (2019) 75–86.
- [36] D. A. Brion, M. Shen, S. W. Pattinson, Automated recognition and correction of warp deformation in extrusion additive manufacturing, *Additive Manufacturing* 56 (2022) 102838.
- [37] Z. Jin, Z. Zhang, G. X. Gu, Autonomous in-situ correction of fused deposition modeling printers using computer vision and deep learning, *Manufacturing Letters* 22 (2019) 11–15.
- [38] Z. Jin, Z. Zhang, G. X. Gu, Automated real-time detection and prediction of interlayer imperfections in additive manufacturing processes using artificial intelligence, *Advanced Intelligent Systems* 2 (1) (2020) 1900130.
- [39] L. Lu, J. Hou, S. Yuan, X. Yao, Y. Li, J. Zhu, Deep learning-assisted real-time defect detection and closed-loop adjustment for additive manufacturing of continuous fiber-reinforced polymer composites, *Robotics and Computer-Integrated Manufacturing* 79 (2023) 102431.

- [40] D. A. Brion, S. W. Pattinson, Generalisable 3d printing error detection and correction via multi-head neural networks, *Nature communications* 13 (1) (2022) 4654.
- [41] A. Tantillo, Annealing of fused filament fabricated nylon 6 with elevated isostatic pressure, Rochester Institute of Technology, 2019.
- [42] M. Sardinha, C. M. Vicente, N. Frutuoso, M. Leite, R. Ribeiro, L. Reis, Effect of the ironing process on abs parts produced by fdm, *Material Design & Processing Communications* 3 (2) (2021) e151.
- [43] Y. Chai, R. W. Li, D. M. Perriman, S. Chen, Q.-H. Qin, P. N. Smith, Laser polishing of thermoplastics fabricated using fused deposition modelling, *The International Journal of Advanced Manufacturing Technology* 96 (2018) 4295–4302.
- [44] J. Etienne, N. Ray, D. Panozzo, S. Hornus, C. C. L. Wang, J. Martínez, S. McMains, M. Alexa, B. Wyvill, S. Lefebvre, Curvislicer: slightly curved slicing for 3-axis printers, *ACM Trans. Graph.* 38 (4) (Jul. 2019). doi: 10.1145/3306346.3323022.
- [45] Y. Li, D. He, S. Yuan, K. Tang, J. Zhu, Vector field-based curved layer slicing and path planning for multi-axis printing, *Robotics and Computer-Integrated Manufacturing* 77 (2022) 102362.
- [46] Y. Chen, T. Zhang, Y. Huang, T. Liu, C. C. Wang, Co-optimization of tool orientations, kinematic redundancy, and waypoint timing for robot-assisted manufacturing, *IEEE Transactions on Automation Science and Engineering* 22 (2025) 12102–12117.
- [47] F. Xie, L. Chen, Z. Li, K. Tang, Path smoothing and feed rate planning for robotic curved layer additive manufacturing, *Robotics and Computer-Integrated Manufacturing* 65 (2020) 101967.
- [48] X. Guidetti, N. Mingard, R. Cruz-Oliver, Y. Nagel, M. Rueppel, A. Rupenyan, E. C. Balta, J. Lygeros, Force controlled printing for material extrusion additive manufacturing, *Additive Manufacturing* (2024).
- [49] J. Fischer, M. Echsel, P. Springer, O. Refle, In-line measurement of extrusion force and use for nozzle comparison in filament based additive manufacturing, *Progress in Additive Manufacturing* 8 (1) (2023) 9–17.

- [50] T. J. Coogan, D. O. Kazmer, In-line rheological monitoring of fused deposition modeling, *Journal of Rheology* 63 (1) (2019) 141–155.
- [51] G. Fang, T. Zhang, Y. Huang, Z. Zhang, K. Masania, C. C. Wang, Exceptional mechanical performance by spatial printing with continuous fiber: curved slicing, toolpath generation and physical verification, *Additive Manufacturing* 28 (2024) 104048.